Research Article

The Development of A Flexible Battery by Using A Stainless Mesh Anode

Kaname Iwai, Teppei Tamura, Dang-Trang Nguyen, Kozo Taguchi[*]

Department of Electrical and Electronic Engineering, Ritsumeikan University, Japan

ABSTRACT. We have developed a compact and flexible battery, which composes three parts: (1) an anode electrode made for stainless mesh which was heat-treated for 30 min at $500℃$ with coated carbon nanotube (CNT), (2) a piece of paper filter-based membrane with the pore size of 0.025 µm and the thickness of 100 µm, and (3) a cathode electrode coated potassium ferricyanide. The battery can generate electricity activated by adding 50 µL sodium chloride (NaCl) solution to the anode. The battery has a NaCl concentration-dependence characteristic. In this research, we tested 0.5, 1, 3, 5, and 10% NaCl solution, respectively. At 3% NaCl concentration, the maximum power density and current density of 42.3 µW/cm² and 228 µA/cm² were obtained, respectively. After the experiments, there was a blue material encountered on the anode surface. By using EDS to analyze the blue material, it could be confirmed that the blue material was ferric ferrocyanide (Prussian blue). The operation principle of this battery was proposed as follows. First, on the anode side, the injected sodium chloride solution oxidizes the stainless mesh surface, then ferric ions and electrons are released. Second, on the cathode side, ferricyanide ions are reduced to ferrocyanide ions by electrons coming from the anode through the external circuit. Simultaneously, ferric ions react with ferrocyanide ions to produce Prussian blue and generate more electrons. This battery can be potentially utilized for applications that require on-demand, disposable, and flexible characteristics. ©2019. CBIORE-IJRED. All rights reserved

Keywords: flexible, stainless mesh, NaCl, Prussian blue, potassium ferricyanide

1. Introduction

The widespread use of flexible electronic devices urgently enhances the requirements for flexible material such as flexible electrodes, separators, and battery packing (Long et al., 2018). Conventional tool steels are widely applied to manufacture cutters and wear-resistant components because of their high hardness, high strength, and well wear resistance. However, corrosion resistance limits their use in certain service environments, such as saline solutions (Wei, Liu, Li, & Cheng, 2019). On the other hand, atmospheric corrosion is characterized by electrochemical degradation of metal in the presence of droplets or thin films of electrolytes (Tang et al., 2019).

Most metallic materials are usually used either in the industry as materials of construction or in medical treatment as orthopedic implant devices, rely on the presence of passive films on their surface to develop good corrosion resistance (Omanovic & Roscoe, 1999). Electrochemical techniques have been widely employed in accelerated corrosion studies (Sousa & Barbosa, 1991). Among the factors influencing corrosion, stress is of vital importance as it accelerates the failure of metals suffering from pitting corrosion (Guo, Wang, & Han, 2018).

It is renown that chloride solutions are among the most aggressively corrosive environments (Kocijan, Milosev, &

Pihlar, 2003). The corrosion rate of steels in neutral NaCl solutions is initiated through two main mechanisms: formation and build-up of a passivating iron oxide layer and partial destruction of this layer by pitting (Scotto, Cintio, & Marcenaro, 1985). It is generally accepted that pitting corrosion is preceded by the appearance of tiny corrosion seeds on the metal surface, which is naturally protected by an oxide layer. At ambient conditions, a thin protective oxide film forms on the surface of mild steel. Unlike that formed on stainless steels, it is not protective in the presence of electrolytes and it usually breaks down (Cáceres, Vargas, & Herrera, 2009). It was found that in 3.5% NaCl solution, the effect of corrosion on the overall cavitation erosion-corrosion was most pronounced in mild steel and grey cast iron and negligible in stainless steel (Kwok, Cheng, & Man, 2000). For example, 3% NaCl solution is equal to the concentration of seawater, 0.5% NaCl is equal to the concentration of NaCl in human sweat. The development of this corrosion product can have a significant effect on the dissolution behavior of the underlying steel (Barker et al., 2019). The steel's performance in oxidizing environments is well established, but its behavior in corrosive environments, particularly those containing sulfiding species and

---

[*] Corresponding author: taguchi@se.ritsumei.ac.jp (Kozo Taguchi)

chlorides have not been studied extensively (Tsaur, Rock, Wang, & Su, 2005).

Stainless steel mesh is low-cost containing mainly iron and can be used as an outstanding flexible substrate after chemical treatment to modify its surface. The metal, iron, can be easily oxidized to Fe_2O_3 (Shinata, Takahashi, & Hashiura, 1987). As one of the common anode materials in energy storage devices, Fe_2O_3 has many advantages, such as low toxicity, low-cost, and high theoretical capacity (Long et al., 2018). The reaction is shown below (Eq. (1)).

$$2Fe + 3H_2O \ \rightarrow \ Fe_2O_3 + 6H^+ + 6e^- \qquad (1)$$
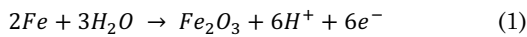
In this paper, we developed a flexible battery with a stainless mesh-based anode. The battery was activated by dropping NaCl solution to the anode. A stable output was obtained for more than one hour. After the operation, there was a blue material that emerged on the anode surface — the blue material was analyzed by energy-dispersive X-ray spectroscopy (EDS).

2. Materials and Methods

2.1 Battery design and materials

The design of the battery is shown in Fig. 1. The battery composed of three main parts: an anode electrode, a membrane, and a cathode electrode.
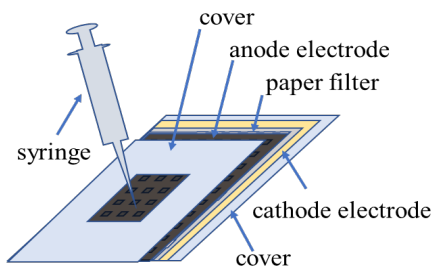
Fig. 1 Battery design

The anode electrode (10 mm $\times$ 10 mm) were made of stainless mesh (PS100-321, HIKARI, Japan), which was heat-treated at 500℃ for 30 min (Fig. 2). After heat-treatment, the color of stainless mesh changed to dark brown color, which is the color of Fe_2O_3. Moreover, it was dip-coated in multiwalled carbon nanotube dispersion solution (CNT, N7006L, KJ Specialty Paper, Japan) for 1 min, and dried at room temperature (Fig. 3). The CNT network provides high conductivity and flexibility (Cui, Hu, Choi, & Cui, 2010).
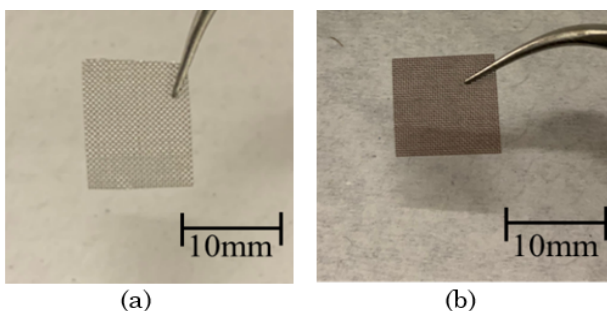
Fig. 2 Photo images of stainless mesh (a) before and (b) after heat treatment
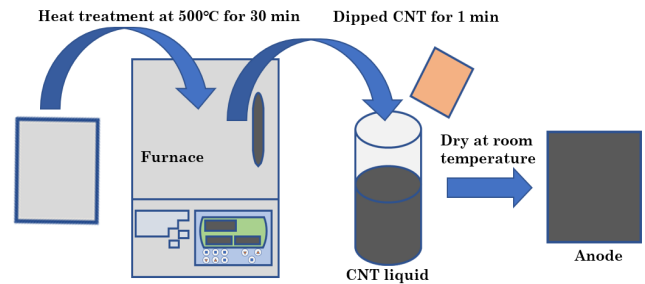
Fig. 3 The process of making the anode electrode

The cathode electrode (10 mm $\times$ 10 mm) was made of hydrophilic carbon sheets and potassium ferricyanide (Wako, Japan). Hydrophilic carbon sheet was dipped into potassium ferricyanide 0.75 M for 1 min and dried at 60℃ for 20 min (Fig. 4). Potassium ferricyanide was used as the electron acceptor at the cathode. The reduction reaction of ferricyanide ions to ferrocyanide ions is as follows (Eq. (2)).

$$[Fe(CN)_6]^{3-} + e^- \ \rightarrow \ [Fe(CN)_6]^{4-} \qquad (2)$$
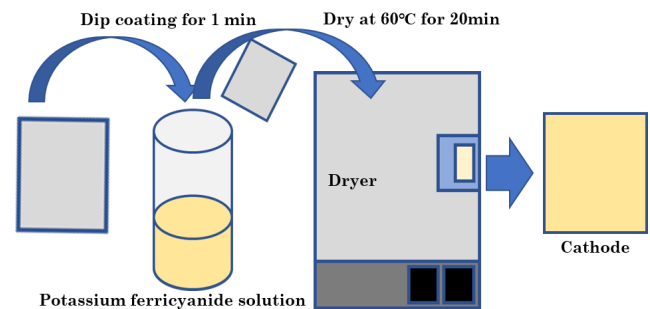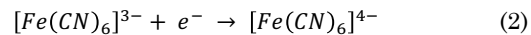
Fig. 4 The process of making cathode electrodes

Paper filter (0.025 μm pore size and 100 μm thickness) (VSWP09025, Merck, Japan) was used to make the paper-based membrane (15 mm $\times$ 15 mm). The flexibility of stainless mesh and the battery is shown in Fig. 5. It can be seen that the battery can be bent easily.

The battery cover was made of silicone rubber (15 mm $\times$ 15 mm $\times$ 2 m) (Monotaro, Japan). On the anode side, the cover was cut a hole (5 mm $\times$ 5 mm) for injecting aqueous sodium chloride solution to the anode to activate the battery.
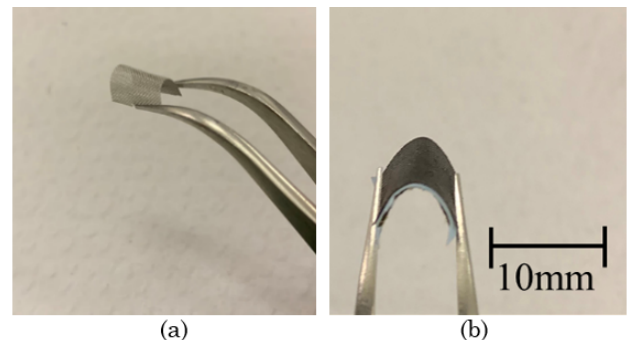
Fig. 5 Flexibility of (a) stainless mesh and (b) the battery without the cover

2.2 Experimental setup

The experimental setup is shown in Fig. 6. An external resistor was connected between the anode and cathode to

discharge the battery. The voltage between the anode and cathode was measured with a data acquisition system (DAQ, National Instrument, USB-6211), and recorded every 30 sec via a customized LabView interface. The current through the resistor was calculated using Ohm's law. To measure the power density curves, we connected respectively 80 kΩ, 50 kΩ, 12 kΩ, 5 kΩ, 2.6 kΩ, 810 Ω, 380 Ω, 150 Ω, and 47 Ω resistors to the external circuit to discharge the battery. The discharging voltage was recorded to calculate the power density. For each experiment, at least three samples were examined, and the average result was used in this paper.
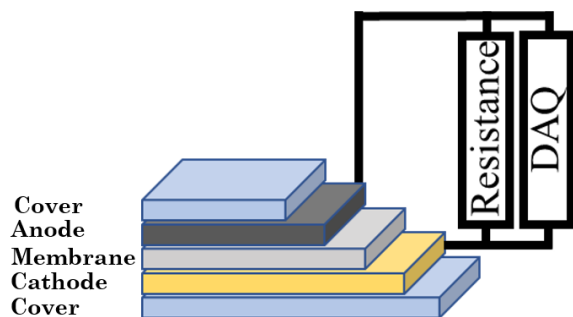
Fig. 6 Experimental setup

3. Results and Discussions

3.1 Blue material on the anode after the experiment

After the experiment, we encountered a blue material on the anode electrode (Fig. 7).
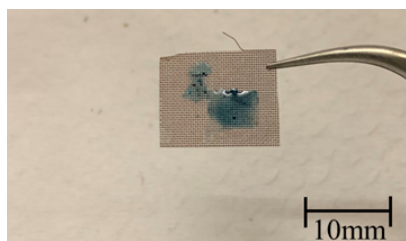
Fig. 7 Photo image of the anode electrode without CNT after the experiment

We suspected that this material was mainly composed of Prussian blue ($Fe_4[Fe(CN)_6]_3$), which is generated from the reaction between Fe_2O_3 and ferrocyanide ions ($[Fe(CN)_6]^{4-}$) as shown in Eq. (3). Prussian blue is usually used in the painting industry.

$$2Fe_2O_3 + 6H_2O + 3[Fe(CN)_6]^{4-} \rightarrow [Fe(CN)_6]_3 + 12OH^- + 12e^- \tag{3}$$
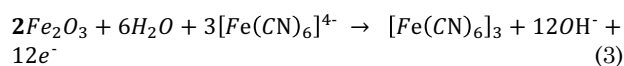
3.2 EDS characterization

To confirm the presence of Prussian blue, we collected the blue material from the anode electrode after the experiment and analyzed it by EDS coupled with scanning electron microscopy (SEM) (SU-1500, Hitachi, Japan). Fig. 8 shows the collected blue material generated on the anode electrode after the experiment. Its elemental composition was analyzed by EDS.
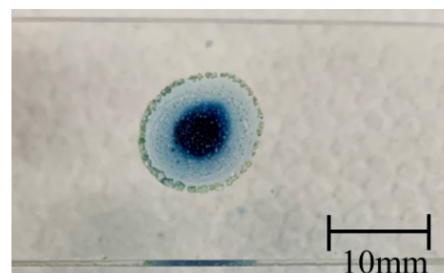
Fig. 8 Photo image of the blue material used for EDS measurement

Fig. 9 (a) shows the SEM image of the blue material. Fig 9 (b) shows the elemental spectrum pattern of the blue material. The qualitative elemental composition is listed in table 1. From these results, it can be confirmed that eight elements existed in the sample. The stainless mesh composed of Fe, Cr, Ni, and O. Prussian blue composed of Fe, C, and N. Furthermore, Na and Cl were originated from the injected saline solution for battery activation. Based on the unique blue color and measured elemental composition of the material, it can be confirmed that there was the existence of Prussian blue in the sample. Therefore, the reaction expressed in Eq. (3) has occurred during the experimental process.
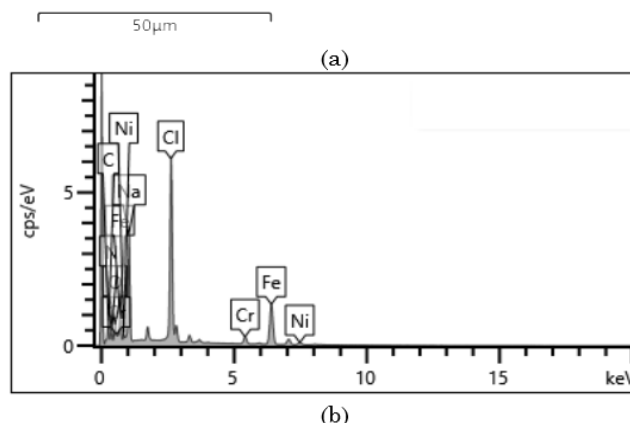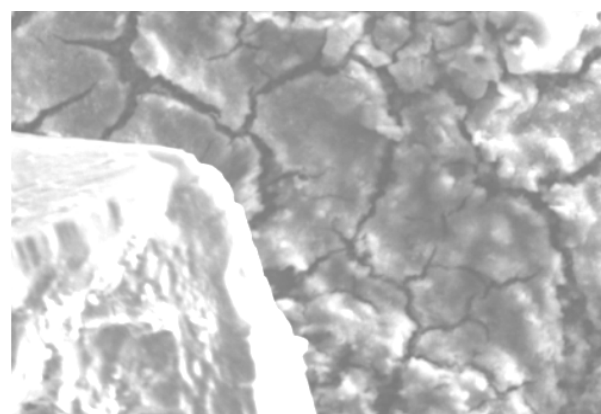
Fig. 9 The SEM image (a) and the elemental spectrum (b) of the blue material

Fig. 10 shows the elemental mapping of the blue material mapped by EDS. From Fig. 10 (g) and (h), there was the presence of NaCl crystal at the lower left.
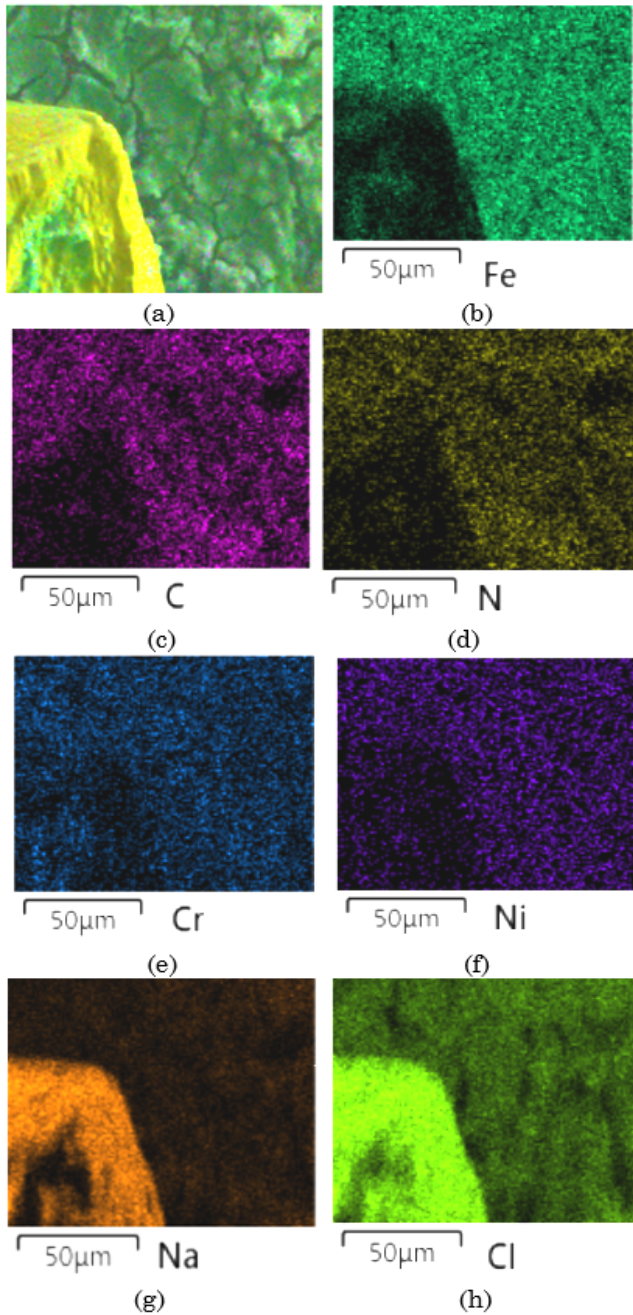
Fig. 10 Elemental mapping of the blue material

Table 1
Elemental composition of the blue material

Element	wt%
C	19.53
N	18.37
O	10.78
Na	15.24
Cl	17.48
Cr	1.85
Fe	15.50
Ni	1.26
Total:	100.00

Prussian blue was generated from the reaction at the anode electrode between **Fe_2O_3** and potassium ferrocyanide ions coming from the cathode electrode (Eq. 3). This reaction is expected to have a positive contribution to the electricity generation of the battery.

3.3 Characteristics of the anode

To justify the operation principle of the battery, we investigated the performance of two types of anode electrodes: (i) heat-treated stainless mesh without CNT coating, and (ii) heat-treated stainless mesh with CNT coating. Fig. 11 displays the discharging voltage (discharged by an 810 Ω resistor) generated by those two anode electrodes. The anode (i) showed a lower output than that of the anode (ii). This result may be attributed to the binding and electron-collecting characteristics of CNT. Thus, the anode (ii) also had a shorter startup time than that of the anode (i). Based on this result, the anode electrode with heat-treatment and CNT coating could produce higher power.

Moreover, the heat-treatment process is necessary for the creation of a layer of Fe_2O_3 on the surface of the stainless mesh. The layer of Fe_2O_3 is important for the reaction in Eq. (3), which produces mainly electricity for the battery.
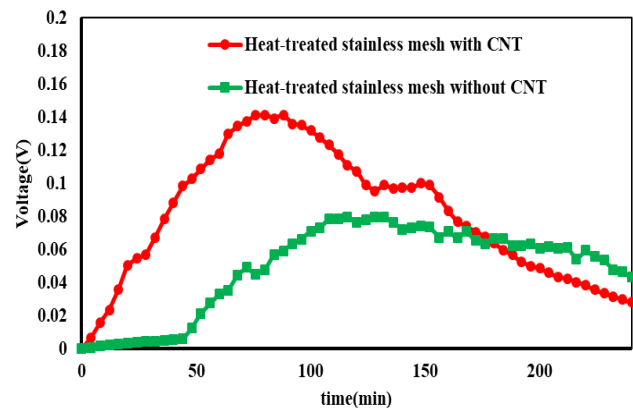
Fig. 11 Performance of two types of anode electrodes

3.4 NaCl concentration and the performance of the battery

In this section, we evaluated the impact of the concentration of the injected NaCl solution on the generated power density of the battery. Five concentrations of NaCl solution (0.5, 1, 3, 5, and 10%) were tested. An appropriate amount of NaCl was dissolved in deionized water to obtain the desired concentration. In this experiment, the anode electrode was heat-treated stainless mesh with CNT. The power density curves are shown in Fig. 12. As the NaCl concentration increased from 0.5 to 3%, the power density increased. However, it decreased when the NaCl concentration increased by more than 3%. This result may be due to NaCl crystal covers up the anode surface faster at higher NaCl concentration. As a result, there is a less active area for the reactions in Eqs. (1) and (3) leading to lower the power density.

Based on this experimental result, 3% was the optimum NaCl concentration. The maximum power density of the battery obtained at 3% NaCl concentration was 42.3 µW/cm² obtained at 810 Ω external resistance.
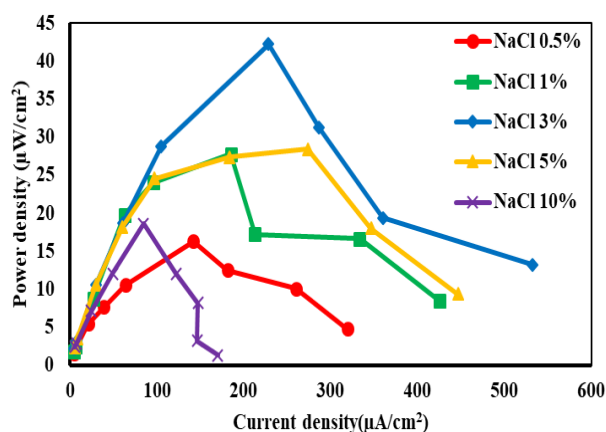
Fig. 12 The power density curves of the battery activated by five NaCl solution concentrations

4. Conclusion

In this paper, we made a flexible battery that used heat-treated stainless mesh with CNT coating as the anode electrode. The operation principle of electricity generation from the creation of Prussian blue on the anode was discussed. The concentration of the injected NaCl solution for activation was also examined. At 3% NaCl concentration, the maximum power density and current density of the battery were 42.3 $\mu W/cm^2$ and 228 $\mu A/cm^2$, respectively. Moreover, the importance of heat-treatment and CNT coating processes of the anode electrode was also investigated.

References

Barker, R., Al Shaaili, I., De Motte, R. A., Burkle, D., Charpentier, T., Vargas, S. M., & Neville, A. (2019). Iron carbonate formation kinetics onto corroding and pre-filmed carbon steel surfaces in carbon dioxide corrosion environments. *Applied Surface Science*, *469*, 135–145. https://doi.org/10.1016/j.apsusc.2018.10.238

Cáceres, L., Vargas, T., & Herrera, L. (2009). Influence of pitting and iron oxide formation during corrosion of carbon steel in unbuffered NaCl solutions. *Corrosion Science*, *51*(5), 971–978. https://doi.org/10.1016/j.corsci.2009.02.021

Cui, L. F., Hu, L., Choi, J. W., & Cui, Y. (2010). Light-weight free-standing carbon nanotube-silicon films for anodes of lithium ion batteries. *ACS Nano*, *4*(7), 3671–3678. https://doi.org/10.1021/nn100619m

Guo, S., Wang, H., & Han, E. H. (2018). Computational evaluation of the influence of various uniaxial load levels on pit growth of stainless steel under mechanoelectrochemical interactions. *Journal of the Electrochemical Society*, *165*(9), 515–523. https://doi.org/10.1149/2.1071809jes

Kocijan, A., Milosev, I., & Pihlar, B. (2003). The influence of complexing agent and proteins on the corrosion of stainless steels and their metal components. *Journal of Materials Science. Materials in Medicine*, *14*(1), 69–77. Retrieved from http://www.ncbi.nlm.nih.gov/pubmed/15348541

Kwok, C. T., Cheng, F. T., & Man, H. C. (2000). Synergistic effect of cavitation erosion and corrosion of various engineering alloys in 3.5% NaCl solution. *Materials Science and Engineering A*, *290*(1–2), 145–154. https://doi.org/10.1016/S0921-5093(00)00899-6

Long, B., Yang, H., Wang, F., Mao, Y., Balogun, M. S., Song, S., & Tong, Y. (2018). Chemically-modified stainless steel mesh derived substrate-free iron-based composite as anode materials for affordable flexible energy storage devices. *Electrochimica Acta*, *284*, 271–278. https://doi.org/10.1016/j.electacta.2018.07.097

Omanovic, S., & Roscoe, S. G. (1999). Electrochemical studies of the adsorption behavior of bovine serum albumin on stainless steel. *Langmuir*, *15*(23), 8315–8321. https://doi.org/10.1021/la990474f

Scotto, V., Cintio, R. Di, & Marcenaro, G. (1985). The influence of marine aerobic microbial film on stainless steel corrosion behaviour. *Corrosion Science*, *25*(3), 185–194. https://doi.org/10.1016/0010-938X(85)90094-0

Shinata, Y., Takahashi, F., & Hashiura, K. (1987). NaCl-induced hot corrosion of stainless steels. *Materials Science and Engineering*, *87*(C), 399–405. https://doi.org/10.1016/0025-5416(87)90404-6

Sousa, S. R., & Barbosa, M. A. (1991). Electrochemistry of AISI 316L stainless steel in calcium phosphate and protein solutions. *Journal of Materials Science: Materials in Medicine*, *2*(1), 19–26. https://doi.org/10.1007/BF00701683

Tang, X., Ma, C., Zhou, X., Lyu, X., Li, Q., & Li, Y. (2019). Atmospheric corrosion local electrochemical response to a dynamic saline droplet on pure Iron. *Electrochemistry Communications*, *101*, 28–34. https://doi.org/10.1016/j.elecom.2019.01.011

Tsaur, C. C., Rock, J. C., Wang, C. J., & Su, Y. H. (2005). The hot corrosion of 310 stainless steel with pre-coated NaCl/Na 2so4 mixtures at 750°C. *Materials Chemistry and Physics*, *89*(2–3), 445–453. https://doi.org/10.1016/j.matchemphys.2004.10.002

Wei, L., Liu, Y., Li, Q., & Cheng, Y. F. (2019). Effect of roughness on general corrosion and pitting of (FeCoCrNi)0.89(WC)0.11 high-entropy alloy composite in 3.5 wt.% NaCl solution. *Corrosion Science*, *146*, 44–57. https://doi.org/10.1016/j.corsci.2018.10.025